

Shaft resistance of bored cast-in-place concrete piles in oil sand – Case study

L. Barr¹ and R.C.K. Wong^{*2}

¹*Department of Civil Engineering, Schulich School of Engineering, University of Calgary, Alberta, Canada*

²*Department of Civil Engineering, 2500 University Drive NW, Calgary, Alberta T2N 1N4, Canada*

(Received December 07, 2011, Revised January 10, 2013, Accepted February 08, 2013)

Abstract. Pile load tests using Osterberg cells (O-cell) were conducted on cast-in-place concrete piles founded in oil sand fill and in situ oil sand at an industrial plant site in Fort McMurray, Alberta, Canada. Interpreted pile test results show that very high pile shaft resistance (with the Bjerrum-Burland or Beta coefficient of 2.5-4.5) against oil sand could be mobilized at small relative displacements of 2-3% of shaft diameter. Finite element simulations based on linear elastic and elasto-plastic models for oil sand materials were used to analyze the pile load test measurements. Two constitutive models yield comparable top-down load versus pile head displacement curves, but very different behaviour in mobilization of pile shaft and end bearing resistances. The elasto-plastic model produces more consistent matching in both pile shaft and end bearing resistances whereas the linear elastic under- and over-predicts the shaft and end bearing resistances, respectively. The mobilization of high shaft resistance in oil sand under pile load is attributed to the very dense and interlocked structure of oil sand which results in high matrix stiffness, high friction angle, and high shear dilation.

Keywords: cast-in-place concrete pile; shaft resistance; Osterberg-cell pile test; shear dilation; oil sand

1. Introduction

Bored cast-in-place concrete piles founded in McMurray Formation oil sand were used to support heavily loaded structures at the extraction and upgrading plant sites in the Fort McMurray area of northern Alberta, Canada since the early 1970's. Results from previous pile load tests conducted on expanded base (belled) piles founded in oil sand indicate that high ultimate end bearing capacity of up to 8 MPa at a depth of less than 15 m could be mobilized (Sharma *et al.* 1986). The shaft resistance between the pile and the oil sand was not investigated and was frequently ignored in the design of such piles in oil sand.

In recent oil sand plant developments, straight shaft cast-in-place concrete piles in oil sand were used in foundation design and construction. As a result, high capacity pile load test programs involving static, Osterberg cell (O-cell) and Statnamic tests were carried out on straight shaft cast-in-place concrete piles founded in oil sand (Clementino *et al.* 2006, 2011). Results of these pile load tests demonstrate that high shaft resistances could be supported in oil sand at relatively

*Corresponding author, Associate Professor, E-mail: rckwong@ucalgary.ca

small shaft displacements, i.e., the pile shaft resistance coefficients could be as high as up to 5. Large end bearing resistances were also attained but at significantly large toe displacements. As a result, recent foundation designs have primarily adopted straight shaft piles founded in oil sand at greater depths as compared to those in previous practices.

Although large shaft resistances have been measured in oil sand, the current state of practice in design of statically loaded cast-in-place concrete piles in granular soils significantly under-predicts these shaft resistances, unnecessarily restricting design capacities. The objective of this paper is to quantify important factors contributing to high shaft resistances measured in straight shaft cast-in-place concrete piles founded in oil sand. The first part of the paper presents pile load test results from the current study. The second part aims at analyzing the pile behaviour interpreted from pile load tests using finite element simulation. Finally, concluding remarks are made based on the numerical modelling.

2. Current case study – Pile load tests

O-cell tests were conducted on three fully instrumented piles (A1, A2, A3) founded in oil sand at a site in the Fort McMurray area of northern Alberta, Canada. The soil conditions at the test site consists of thin glacial deposits (outwash sand, lacustrine clay, and glacial clay till) overlying upper and/or Middle McMurray Formation oil sand. Overburden soils were removed and the test piles were installed directly through small amounts of oil sand fill into the underlying in situ oil sand. The McMurray Formation is characteristically uncemented, with exception of occasional indurated siltstone layers. The sands of the McMurray Formation are approximately 90-95% quartz and are 99% water-wet (Carrigy 1966). The interstitial space may contain any of water, bitumen and gas. Bitumen contents, defined as the mass of bitumen divided by the total mass of the sample, ranged from 3% to 12% at the test locations. However, most of the samples obtained from the upper 3 m of the McMurray Formation indicated lean oil sand (i.e., less than 6% bitumen content).

Table 1 presents a summary of the test pile characteristics including test pile dimensions, test method, and soil stratigraphy. Test pile A1 was a straight shaft pile, and test pile A3 had a belled base. These two piles were relatively long and embedded in various different formations, and thus multi-stage O-cell tests were used to measure the shaft resistances at various depth intervals. Test pile A2 was a straight shaft pile, and single-stage O-cell test was conducted to delineate its capacity. An O-cell consists of a specially designed hydraulic jack capable of exerting very large loads at high internal pressures. In single-stage test, the O-cell is typically placed on or near the bottom of the pile and, when pressurized internally, applies an equal upward and downward load, thus imparting the shaft resistance and the end bearing load. In a multi-stage test, a second O-cell is placed at a predetermined distance up from the bottom of the pile. With this configuration, the shaft resistance of the pile above and below the upper cell along with the end bearing can be estimated. The unit end bearing resistance is usually estimated assuming that the shaft resistance on the portion of the shaft between the O-cell and pile base is equal to the shaft resistance on the portion of the shaft immediately above the O-cell.

Because of its simple pile configuration and embedded soil profile, the load test on test pile A2 was selected for detailed analysis and its results are presented in this paper. Test pile A2 was a straight shaft cast-in-place concrete pile with a 0.75 m nominal diameter and an embedment depth of 10 m. The stratigraphy at this site consisted of dense oil sand fill of 4.6 m in thickness over

Table 1 Pile load tests installation summary (Barr 2011)

Test pile	Stratigraphy	Oil content ^a	Shaft dia. in oil sand ^b (mm)	Pile depth (m) ^c	Type of test
A1 ^b	0 to 4.7m – oil sand fill > 4.7m – oil sand	Lean to rich	1200	18.1	Multi-stage O-cell
A2	0 to 4.6m – Oil sand fill > 4.6m – Oil sand	Lean to rich	750	10.0	Single-stage O-cell
A3	0 to 2.8m – Oil sand fill > 2.8m – Oil sand	Lean to rich	910 shaft, 1200 bell	13.6	Multi-stage O-cell

^aOil content: lean < 6%; moderate 6-8% and rich > 8%

^bBracket values refer to nominal shaft diameter of cased section

^cBracket values refer to length of cased pile section

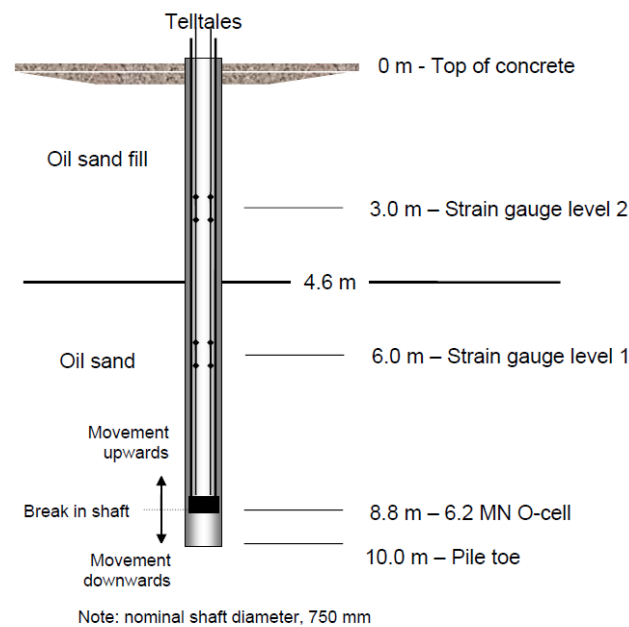


Fig. 1 Pile load test configuration for test pile A2

dense in situ oil sand, with a water table near the surface. The oil sand consisted of fine-to medium-grained sand, with a bitumen content ranging from 0% to 15% over the shaft, and averaging around 6%. Fig. 1 shows a schematic of the pile load test, instrumentation setup, and soil profile. A 405-mm diameter O-cell was installed at a distance of 1.34 m above the pile base. The cell expansion was measured by three linear vibrating wire displacement transducers (LVWDTs) positioned between the lower and upper plates of the O-cell assembly. A pressure gauge and a vibrating wire pressure transducer were used to measure the pressure applied to the O-cell at each load interval. Two vibrating wire strain gauges arranged diametrically were installed at two levels (3-m and 6-m depths) in the pile to measure the compressive strains at the pile sections above the O-cell assembly. The pile compression was measured using the LVWDTs mounted to the 6-mm tell-tales installed in the 13-mm tell-tale steel casings which were attached

to the top of the O-cell assembly extending to beyond the top end of the concrete pile. Two automated digital survey levels were used to monitor the displacement at the top of the pile during testing.

The single-stage O-cell load test was conducted by pressurizing the O-cell in 10 load increments to 40.68 MPa resulting in a bi-directional gross O-cell load of 3.78 MN. The loading was halted when the upper portion of the pile shaft was displacing rapidly and no additional loading was possible. The O-cell was then depressurized in four decrements and the test was concluded. The load was applied in increments according to the Quick Load Test Method for Individual Piles (ASTM 2007), i.e., holding each successive load increment constant for eight minutes.

Fig. 2 presents the applied O-cell load versus cell displacement plot. The cell upward and downward displacements were calculated from the cell expansion and change in level of the tell-tales. A non-linear hardening behaviour was observed both in the upper and lower portions of the pile upon the primary loading. Non-recoverable displacements were detected after unloading. The lower portion yielded a stiffer response than the upper one both in the primary loading and unloading. The load applied by the O-cell acted in two opposing directions, and was resisted by the capacities of the pile above and below. Theoretically, the O-cell does not impose an additional upward load until its expansion force exceeds the buoyant weight of the pile above the O-cell.

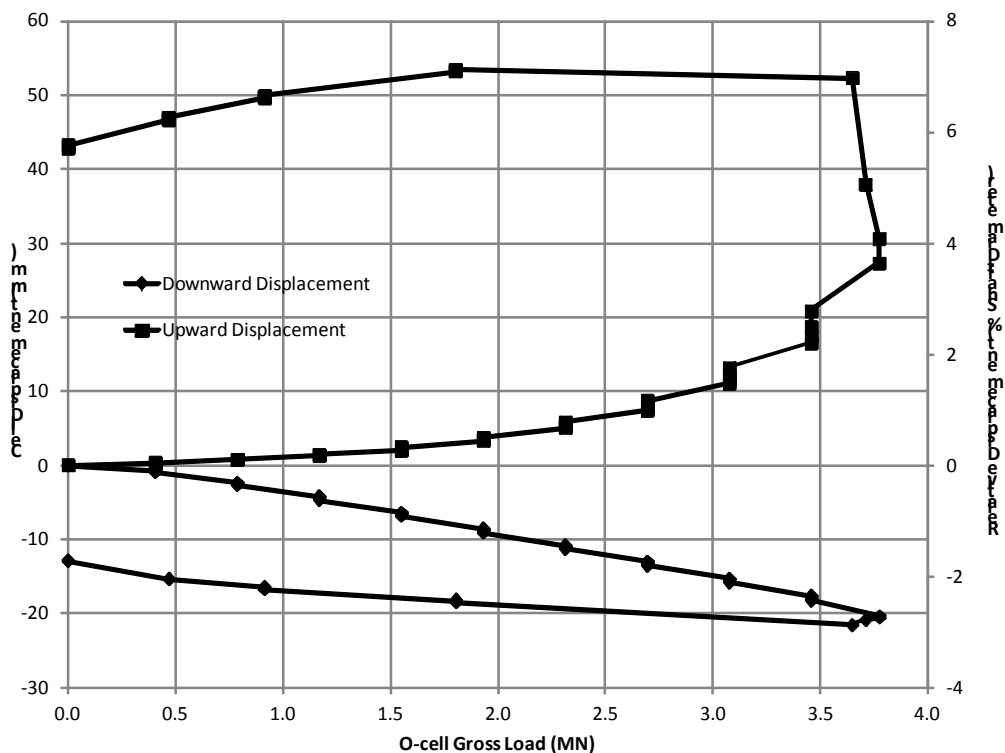


Fig. 2 Load-cell displacement curve of O-cell test in test pile A2. The cell displacement was calculated from the cell expansion and the displacement of the cell top monitored by the tell-tales attached to the cell top

Therefore, *net load*, which is defined as the gross O-cell load minus the buoyant weight of the pile above, is used to determine the shaft shear resistance above the O-cell and to construct the equivalent top-down load settlement curve. A buoyant weight of pile of 0.09 MN above the O-cell was estimated and used in the data analysis.

From Fig. 2, the maximum upward applied *net load* to the upper shaft resistance was 3.70 MN. At this load, the upward displacement of the O-cell top was 31 mm. In order to estimate the shaft shear resistance of the test pile, loads at two strain gauge elevations were calculated based on the strain gauge data and an estimate of pile stiffness, AE (where A is the cross-sectional area of the pile and E is the Young’s modulus of the concrete) of 11,150 MN above the O-cell, and 10,660 MN below the O-cell. The difference in the loads between each elevation was the load taken by the shaft resistance in between (Osterberg 1984, 1998). The average mobilized shaft resistance was determined by dividing the shaft load or resistance by its exposed area.

The average mobilized shaft resistance as a function of the pile displacement in the oil sand fill and in situ oil sand zones were plotted in Figs. 3 and 4, respectively. Effect of pile elastic shortening was not considered in these two figures. The 4.5-m interval or zone represents the oil sand layer between strain gauge levels 1 (at 3 m) and 2 (at 6 m); the 7.5-m interval or zone represents the oil sand layer between the strain gauge level 2 (at 6 m) and the O-cell location (at 8.8 m). At both intervals, the shaft resistance increased with increasing pile displacement

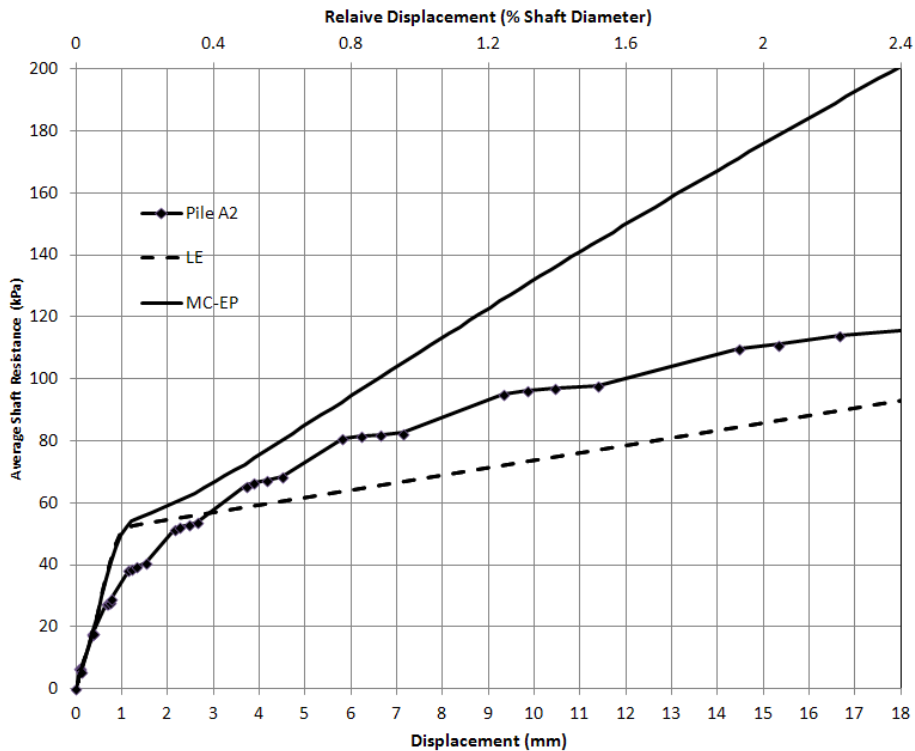


Fig. 3 Interpreted and predicted mobilized shaft resistance versus pile displacement at depth interval between 3 m and 6 m (oil sand fill) in test pile A2 (LE: linear elastic analysis; MC-EP: elasto-plastic analysis)

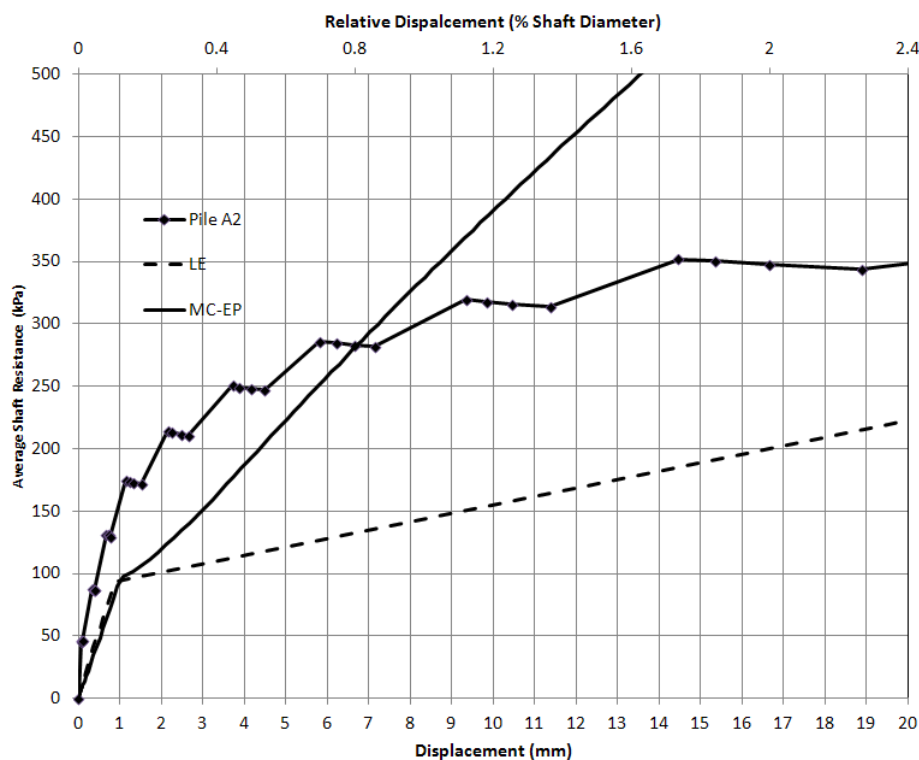


Fig. 4 Interpreted and predicted mobilized shaft resistance versus pile displacement at depth interval between 6 m and 8.8 m (intact oil sand) in test pile A2 (LE: linear elastic analysis; MC-EP: elasto-plastic analysis)

following a hardening behaviour. The increase in the shaft resistance is significant for the initial displacement of about 1–2 mm. The maximum mobilized Bjerrum-Burland coefficient (Burland 1973) or Beta-coefficient (defined as the mobilized shear stress divided by the vertical effective stress) for the oil sand fill and in situ oil sand are 2.5 and 4.5, respectively. The oil sand fill is a backfill material, and its compacted density is lower than that at the intact state, resulting in a lower Beta-coefficient. However, these values for both oil sand fill and intact oil sand are still significantly higher than the typical Beta-coefficients of 0.3–0.9 recommended by ASCE (1984), API (2002) and CGS (2006). They are also higher than those Beta-coefficients measured in model displacement piles in sand (Lehane and White 2005) and pull-out tests on buried steel pipes in compacted Fraser River sand (Wijewickreme *et al.* 2009). Both research groups explained that the Beta-coefficient was increased from its initial value of 0.4 to a fully mobilized value of 2.2 due to the constrained shear-induced dilation of the dense sand near the pipe-sand interface.

From Fig. 2, the maximum load exerted by the O-cell against the combined lower shaft resistance and end bearing was 3.78 MN. At this load, the downward displacement of the O-cell base was 21 mm. The shaft resistance induced in the 1.34-m pile section below the O-cell was calculated to be 1.53 MN assuming an estimated unit shaft shear resistance of 500 kPa and a nominal 750-mm pile diameter. The 500-kPa value was obtained from Fig. 4, i.e., linearly extrapolating the measured shear resistance at the interval between the O-cell and strain gauge

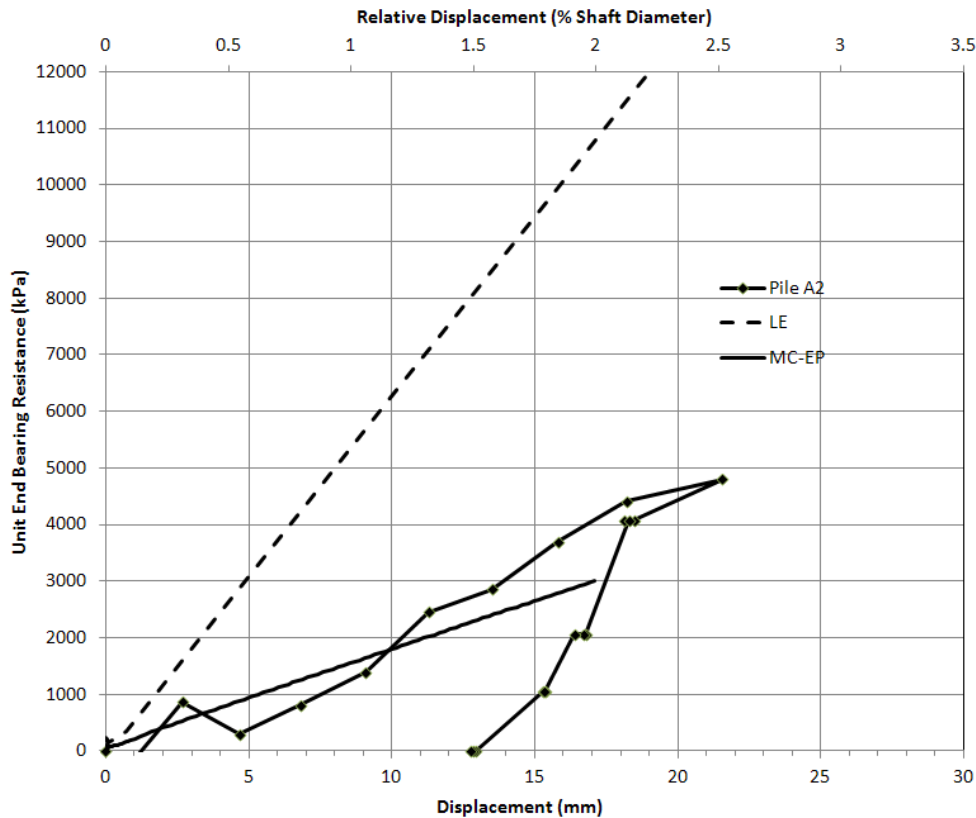


Fig. 5 Interpreted and predicted mobilized unit end bearing resistance versus pile toe displacement in test pile A2 (LE: linear elastic analysis; MC-EP: elasto-plastic analysis)

level 1 at a displacement of 21 mm and assuming a linear distribution of shaft resistance with depth. The applied load to the end bearing was then 2.12 MN and the unit end bearing resistance at the base of the pile was calculated to be 4.8 MPa at the above noted displacement. The unit end bearing resistance versus pile displacement for test pile A2 is presented in Fig. 5. The results indicate that the end bearing resistance was mobilized at the start of the loading or displacement, i.e., relatively little or no disturbance in the base was observed. The end bearing resistance increased with the toe displacement and showed no indication of failure, which is consistent with those observed by Fellenius (1999, 2009) and Veiskarami *et al.* (2011). The maximum mobilized end bearing capacity was about 4.8 MPa at the depth of 10 m. The maximum mobilized end bearing factor N_f defined as the end bearing resistance normalized by the vertical effective stress, is about 44. This value is less than the range of 50-100 recommended for dense sand in CGS (2006) because the test pile has not attained its ultimate end bearing capacity.

The pile top-down load versus pile displacement relationship was determined using the interpretation method described in Lee *et al.* (2008). This method assumes that the shaft resistance along the pile linearly increases with depth, i.e., triangular stress distribution. For the case of rigid pile, an arbitrary pile toe displacement and its corresponding end bearing resistance were selected from Fig. 5. Then, the shaft shear resistances at the lower and upper intervals were interpolated

from Figs. 3 and 4, respectively with the corresponding pile displacement. The corresponding load in the pile head is the summation of end bearing, lower and upper shaft resistances. The above steps were repeated to construct the entire pile top-down load versus pile displacement curve. For the case of elastic pile, the pile elastic shortening due to the pile load must be taken into account. The net displacement of the pile is the summation of elastic shortening of the shaft and the settlement of pile toe. Fig. 6 presents the interpreted pile top-down load versus pile head displacement for pile A2 for cases of rigid pile and elastic pile with the elastic compression correction. The pile displays a non-linear function. The elastic pile has a vertical load capacity of 7.2 MN at a displacement of 25 mm. It appears that the pile did not reach its ultimate resistance based on typical failure criteria. For example, Terzaghi (1943) suggested that the ultimate resistance should be achieved when the pile displacement is equal to 10% of the base (shaft) diameter. From Fig. 5, the pile does not show any sign of yielding in the end bearing resistance. At a pile displacement of 10% of the base (shaft) diameter or 75 mm, the end bearing resistance of 12-15 MPa could be attained depending on the choice of evaluation method, e.g., Davisson's method, Brinch-Hansen's criterion, Chin-Kondner extrapolation limit load and De Beer's method.

To gain a better understanding of the behaviour of the test pile, the load distribution along pile depth for selected load increments were constructed using the above interpretation method, and shown in Fig. 7. The end bearing resistances at 4- and 7.2-MN load increments are about 0.5 and 1.4 MN (10% and 18% of total pile load), respectively. This behaviour indicates the pile capacity in oil sand is dominated by the pile shaft resistance at small displacements. The end bearing

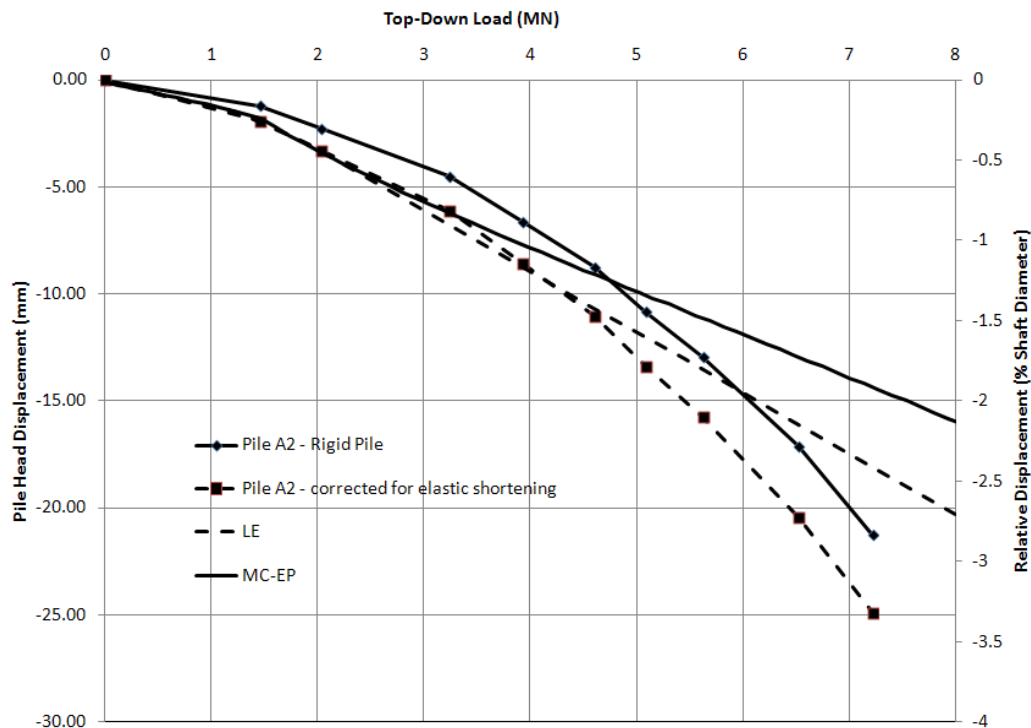


Fig. 6 Interpreted and predicted top-down load versus pile head displacement in test pile A2 (LE: linear elastic analysis; MC-EP: elasto-plastic analysis)

resistance is only fully mobilized at large displacements, and its maximum value is limited to about 3.5 MN for pile A2 if 8-MPa bearing capacity is assumed.

The above interpretation was also conducted on the multi-stage O-cell tests on test piles A1 and A3 (Barr 2011). It was found that the maximum recorded mobilized Beta-coefficient for these two piles in situ oil sand are as high as up to 5.3, and the maximum mobilized end bearing capacity in the belled base was 8.5 MPa. This finding confirms that cast-in-place concrete piles founded in oil sand have uniquely high shaft and end bearing resistances.

3. Back analysis of interpreted behaviour of Test Pile A2

Finite element simulation program (ABAQUS 2009) was used to study the complex pile-oil sand interaction problem. Ideally, all the material constitutive models are developed from the laboratory element tests and implemented in the FE model. Then, “forward” prediction by the FE should be conducted by varying the material parameters within the expected ranges. This approach enhances the predictive capacity of the FE model for future design. Due to the limiting test data on

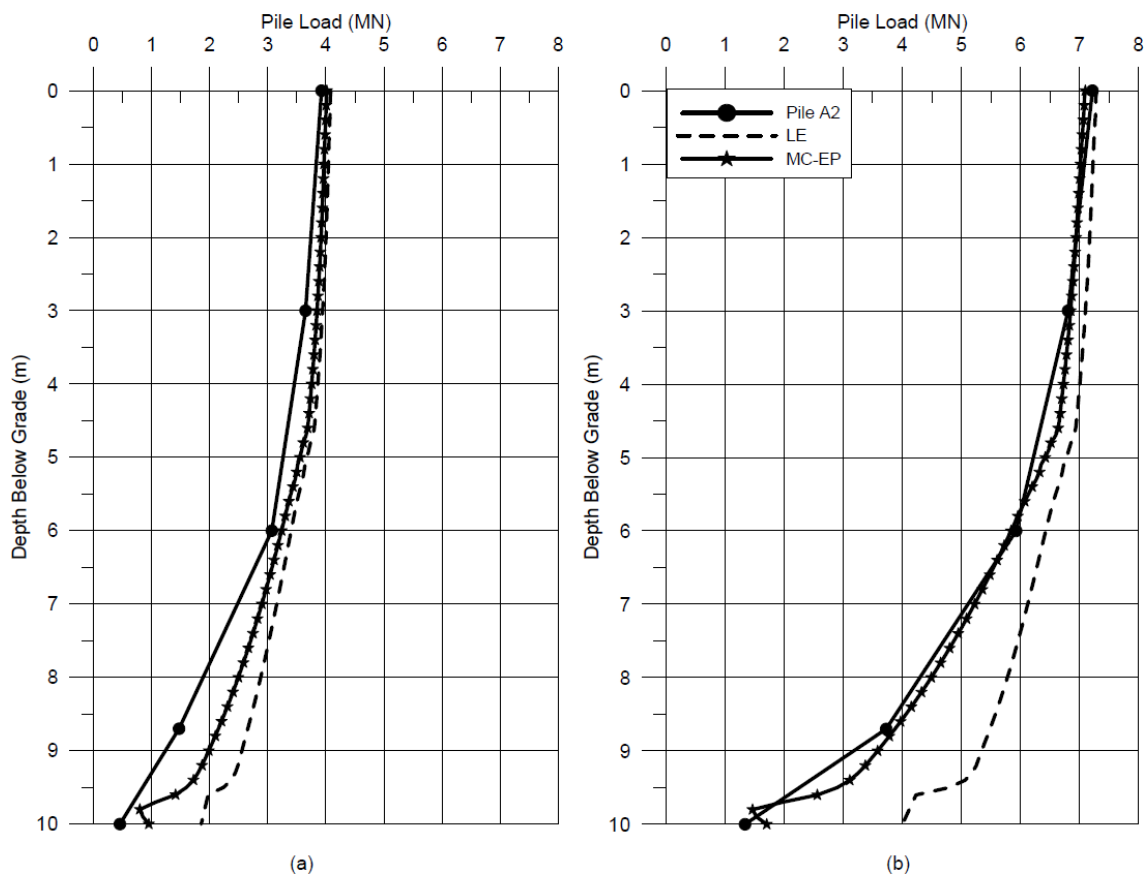


Fig. 7 Interpreted and predicted mobilized shaft resistance versus pile embedment depth for pile head load of (a) 4 MN and (b) 7.2 MN in test pile A2 (LE: linear elastic analysis; MC-EP: elasto-plastic analysis)

the oil sand fill and intact oil sand from this specific site, the objective of the numerical study in this paper is limited to investigate important factors contributing to high shaft resistances measured in straight shaft cast-in-place concrete piles founded in oil sand. These factors include oil sand stiffness, shear strength, shear dilation, interface friction, and in situ stress. Effects of these factors on the pile capacity were studied using linear and non-linear FE analyses (Barr 2011). In here, results of linear elastic and elasto-plastic FE analyses are presented for illustration.

3.1 Constitutive model for oil sand

Various studies were conducted to quantify the engineering behaviour of oil sands, particularly with regards to the shear strength and deformation characteristics.

Sobkowicz and Harris (1977), Dusseault and Morgenstern (1978) and Agar *et al.* (1987) reported peak friction angles ranging between 56° and 61°, and residual friction angles of 30°-35° at confining stresses of 62-1452 kPa. These authors showed that, unlike typical dense quartz sands, oil sand has a large number of concavo-convex and straight (or long) contacts. The high friction angle of oil sand in its undisturbed state is attributed to such interlocked structure resulting from recrystallization of the sand grains under high stress deposition (Dusseault and Morgenstern 1979). Sharma *et al.* (1986) recorded standard penetration test (SPT) values of 103-117 in oil sand at a depth of 10-12 m. These high SPT values indicate that in situ oil sand is a very dense and stiff material.

Samieh and Wong (1997, 1998) and Wong (1999) carried out an extensive study on the strength and deformation characteristics of oil sand at low confining stresses of 5-750 kPa using drained triaxial compression tests. They showed that oil sand exhibits an increase in peak and residual shear strengths with a decrease in confining stress. Severe post-peak strain softening is associated with significant shear dilation. The dilation rate (defined as the ratio of volumetric strain rate to axial strain rate) increases with decreasing confining stress. Non-homogeneous shear deformation occurs at large deformation after the peak strength. Measured peak friction angles lie in a range of 45°-60°. The maximum dilation rates occur with a range of 2-4 at the peak strength, depending on the confining stress. This dilation rate is very high as compared to those of less than unity observed in dense sands reported by Rowe (1962) and Bolton (1986). The high dilation rate in oil sand is attributed to its dense interlocked structure.

A modified Mohr-Coulomb plasticity model, available in ABAQUS (2009), was chosen to capture the elasto-plastic and shear dilative behaviour of the oil sand under pile loading. The model follows the Mohr-Coulomb type failure envelope with smooth corners proposed by Menetrey-Willam (1995). The Mohr-Coulomb criterion assumes that failure occurs when the shear stress on any point in a material reaches a value that depends linearly on the normal stress in the same plane. The Mohr-Coulomb model is based on plotting Mohr's circle for states of stress at failure in the plane of the maximum and minimum principal stresses. For general states of stress, the model is more conveniently written in terms of three stress invariants, friction angle (ϕ) and cohesion (c) as

$$F = R_{mc}q - p \tan \phi - c = 0 \quad (1)$$

where

$$R_{mc}(\Theta, \phi) = \frac{1}{\sqrt{3} \cos \phi} \sin \left(\Theta + \frac{\pi}{3} \right) + \frac{1}{3} \cos \left(\Theta + \frac{\pi}{3} \right) \tan \phi \quad (2)$$

and, Θ equals the deviatoric polar angle defined as

$$\cos(3\Theta) = \left(\frac{r_d}{q} \right)^3 \quad (3)$$

The mean equivalent pressure stress, p , Mises equivalent stress (deviatoric stress), q , and third invariant of deviatoric stress, r_d , are defined as

$$p = -\frac{1}{3} \text{trace}(\sigma) \quad (4)$$

$$q = \sqrt{\frac{3}{2} (S : S)} \quad (5)$$

$$r_d = \left(\frac{9}{2} S \cdot S : S \right)^{\frac{1}{3}} \quad (6)$$

where S is the stress deviator, defined as $S = \sigma + pI$ (I is the Kronecker delta).

The flow potential, G , was chosen as a hyperbolic function in the meridional stress plane and the smooth elliptic function proposed by Menétrey and Willam (1995) in the deviatoric stress plane

$$G = \sqrt{(\epsilon c|_0 \tan \psi)^2 + (R_{mv} q)^2} - p \tan \psi \quad (7)$$

where

$$R_{mv}(\Theta, e) = \frac{4(1 - e^2) \cos^2 \Theta + (2e - 1)^2}{2(1 - e^2) \cos \Theta + (2e - 1) \sqrt{4(1 - e^2) \cos^2 \Theta + 5e^2 - 43}} R_{mc} \left(\frac{\pi}{3}, \phi \right) \quad (8)$$

and

$$R_{mc} \left(\frac{\pi}{3}, \phi \right) = \frac{3 - \sin(\phi)}{6 \cos \phi} \quad (9)$$

where ψ is the dilation angle measured in the p - $R_{mv}q$ plane at high confining pressure; $c|_0$ is the initial cohesion yield stress, $c|_0 = c|_s^{pl} = 0$, which is a user input piecewise function selected to match the strain softening response of the soil in triaxial test conditions; ϵ is a parameter, referred to as the meridional eccentricity, that defines the rate at which the hyperbolic function approaches the asymptote; and e is a parameter, referred to as the deviatoric eccentricity, that describes the “out-of-roundedness” of the deviatoric section in terms of the ratio between the shear stress along the extension meridian ($\Theta = 0$) and the shear stress along the compression meridian ($\Theta = \pi / 3$). The parameter, e , is calculated as

$$e = \frac{3 - \sin \phi}{3 + \sin \phi} \quad (10)$$

This flow potential, which is continuous and smooth, ensures that the flow direction is always uniquely defined. Flow in the meridional and deviatoric stress plane is non-associated in the model, i.e., the flow rule of the plastic potential is non-associative. Prior to yielding, linear elasticity is assumed. Post-peak softening is captured using the cohesion yielding function generated by a user-defined piecewise input available in ABAQUS, which matches the post-peak softening response of oil sand observed in the drained triaxial tests. The rate of the volumetric shear dilation is defined by the dilation angle. Details of formulation on failure criterion, yield function and plastic potential can be found in ABAQUS (2009).

Results of selected drained triaxial compression tests conducted by Samieh and Wong (1997) were modeled using ABAQUS (2009) to demonstrate the adequacy of the model to capture the behaviour of oil sand. Results of two tests at effective confining stresses of 50 kPa and 100 kPa were selected to cover the stress levels encountered in the pile test site. It is important to note that in the modified Mohr-Coulomb plasticity model the material parameters such as Young's modulus, Poisson's ratio, peak friction angle, maximum yield cohesion, and dilation angle are independent of confining stress. In order to match the triaxial test results at varying confining stresses, these parameters embedded in the plasticity model have to be varied, Table 2 provides the values of the material parameters used in the matching.

Fig. 8 compares the laboratory test results with those predicted by the plasticity model. The 50-kPa and 100-kPa samples yield peak friction angles of 59° and 56° along with maximum dilation rates of 2.3 and 2.1, respectively. The model predicts behavioural responses consistent with the laboratory observation. However, there are some limitations in the plasticity model. The model assumes that the Young's modulus and the dilation rate are constant independent of the confining stress. However, the oil sand material displays a stress-dependent modulus and non-linear stress-strain response prior to yielding. In addition, the shear dilation initiates at a pre-peak state, attains its maximum dilation rate at the peak strength state, and decreases gradually to the critical state of zero dilation rate with shearing. Results of Fig. 8 illustrates that the modified Mohr Coulomb model provided in ABAQUS offers a reasonable matching to the response of oil sand in drained triaxial compression tests prior to the peak strength. There are discrepancies in post-peak softening responses. It is shown later in this study that the deformations or strains induced by the pile load are small within the pre-peak strength regime, and post-peak deformations are very limited to small local areas. In addition, localized shear bands were observed in the tests yielding non-unique post-peak behavior.

3.2 Model for concrete pile-oil sand interface

ABAQUS (2009) provides a formulation for modeling finite sliding interaction between two deformable bodies. The pile-soil interaction was simulated by the element-based surface-to-surface (master-slave relationship) contact pair interaction with a Coulomb frictional contact law for sliding. The more rigid pile body, which was chosen as a master surface, was in contact with the more deformable soil, which was selected as a slave surface. Contact conditions between the two surfaces are governed by kinematic constraints in the normal and tangential directions. The normal stress at contact is either zero when there is a gap between the pile and the soil, or compressive when the pile is in contact with the soil. The gap cannot be negative because interpenetration of materials is not allowed. As the master surface moves past the deformable slave surface, the shear and normal forces across this interface are computed. The maximum shear stress at the interface is proportional to the normal stress at the interface. When the shear stress is less than this maximum

Table 2 Material parameters for matching results of triaxial compression tests on oil sand

Confining pressure, σ_3 , (kPa)	50	100
Peak effective friction angle, ϕ' (degrees)	54	55
Maximum yield cohesion, c (kPa)	30	15
Dilation angle, ψ , (degrees)	50	50
Young's modulus, E , (kPa)	100,000	110,000
Poisson's ratio, ϕ	0.47	0.44

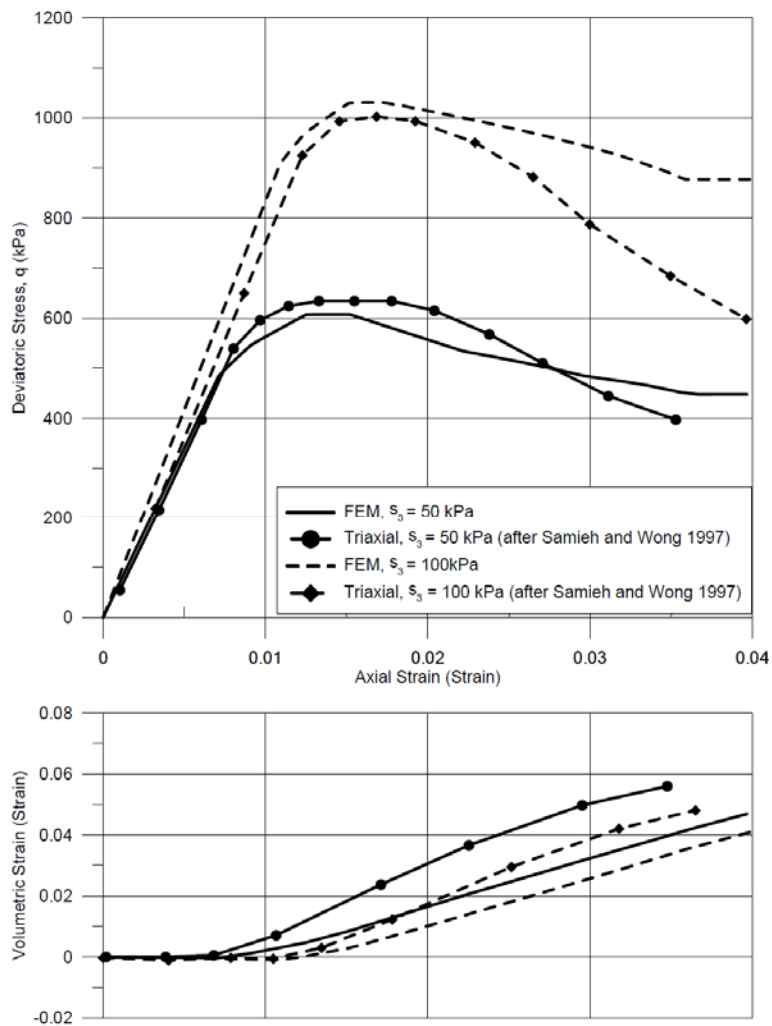


Fig. 8 Measured and predicted response of drained triaxial compression in oil sand

value, sliding takes place in the direction of the shear stress. Note that the surface interaction does not exhibit dilation or volume change itself, but merely connects the two deformable bodies to each other. The constitutive model of the soil is what exhibits dilation. The stiffness method used

for friction is a penalty method that permits some relative motion of the surfaces (an “elastic slip”) when they should be sticking. While the surfaces are sticking, the magnitude of sliding is limited to this elastic slip, F_f .

A series of shear tests were modeled to confirm that the pile-soil interface interaction appropriately captures the normal-shear stress response of the interface. Fig. 9 provides the FEM results of two direct shear tests at normal stresses of 100 kPa and 200 kPa, using coefficients of friction (i.e., $\tan(\delta)$) of 0.8 and 1.1, respectively. As discussed previously, an allowable elastic slip, F_f is used when modeling the stick conditions prior to slipping, with a program default value of 0.005 (5 mm). The default value was thought to allow for too much displacement prior to slip, and therefore a smaller value of 0.0001 (0.1 mm) was used. The pile-oil sand interface displays elastic perfectly plastic behaviour (Fig. 9).

3.3 Finite element model for test pile A2

Since the cast-in-place concrete pile is cylindrical, an axisymmetric model was selected. Fig. 10 shows the finite element mesh of the model. The model consists of 306 pile elements and 5806 soil elements, both 4-noded bilinear quadrilateral solid continuum elements with reduced integration option (ABAQUS 2009).

Roller-type displacement boundary conditions were applied along the vertical sides and base of the finite element mesh. The top surface was allowed to deform freely. The boundary conditions were placed sufficiently far away from the pile to minimize the boundary effects, the base being two times the depth of the pile below grade and approximately 40 times the pile radius laterally

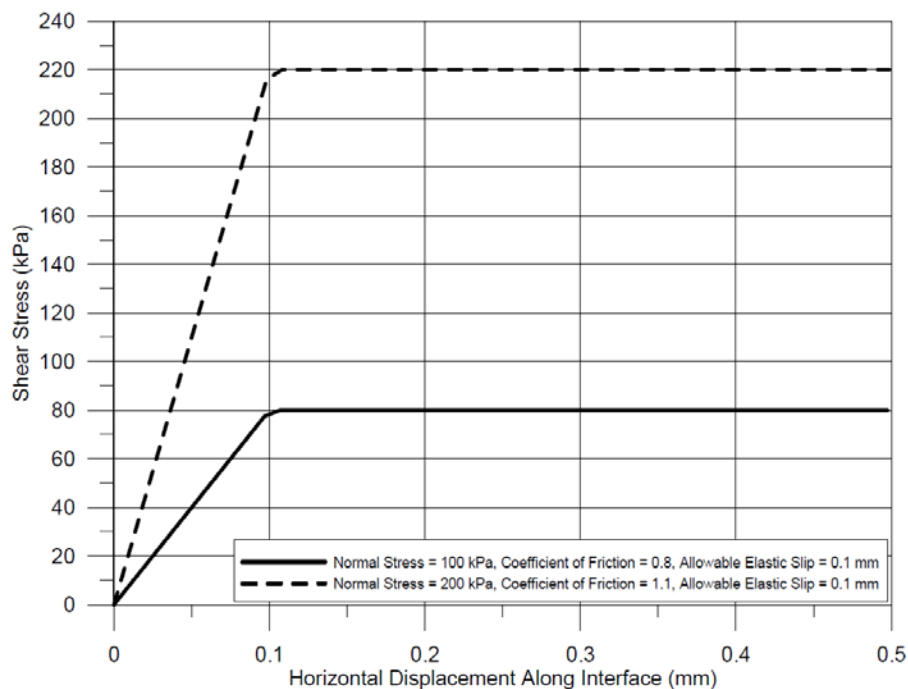


Fig. 9 Response of the interface between the concrete pile and oil sand subject to direct shearing

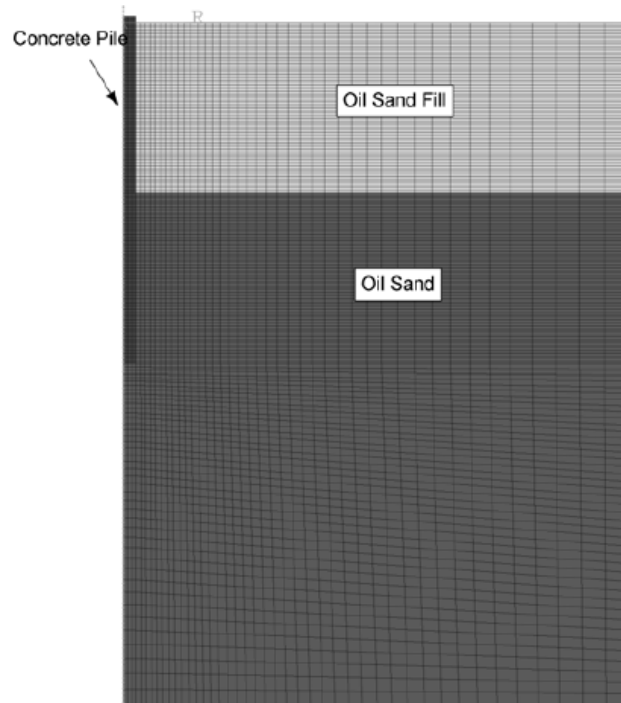


Fig. 10 Finite element mesh for test pile A2

away from the pile. This is consistent with the recommendations provided by Eigenbrod *et al.* (2005) and Said *et al.* (2009). The water table was close to the ground surface. Since the effective permeability to water in lean and rich oil sands were high and the loading rate was small, it was assumed that the pore pressure remained unchanged or the dissipation of the induced excess pore pressure was rapid. Thus, coupled pore pressure/stress, i.e., consolidation analysis was not conducted.

As shown in Figs. 1 and 10, two soil layers consisting of oil sand fill and in situ oil sand were modeled with varying strength, deformation and interface properties. For convenience, the boundary between the fill and in situ oil sand was taken at 5 m below grade. Table 3 lists the soil parameters and other properties used in the finite element simulations presented in this paper. This specific set of input parameters was obtained from finite element parametric studies varying the parameter values within the expected ranges (Barr 2011). The strength-deformation parameters such as Young's modulus, Poisson's ratio, peak friction angle, maximum yield cohesion, and dilation angle were based on the result matching shown in Fig. 8. As the interlocked structure of oil sand would be destroyed in the oil sand fill material, the Young's modulus and dilation angle of the fill material were expected to be lower than those observed in the triaxial compression tests. For the in situ oil sand, a higher value in Young's modulus was used for modelling because some degree of sample disturbance was expected to be encountered in sample coring and trimming for triaxial compression tests (Dusseault and Morgenstern 1978). The coefficient of lateral earth pressure at-rest was chosen to be unity as Athabasca oil sand formation is heavily overconsolidated (Dusseault 1978, Bawden 1983). The mechanical properties for the concrete pile are the typical

Table 3 Model parameters for oil sand fill and intact oil sand used in finite element simulation

Material	Property	Value	Units
Oil sand fill	Young's modulus	100E3	kPa
	Poisson's ratio	0.47	
	Buoyant unit weight	11	kN/m ³
	Maximum initial yield cohesion	15	kPa
	Mohr-Coulomb peak friction angle	45	degrees
	Dilation angle	20	degrees
	Initial coefficient of lateral earth pressure	1.0	
Oil sand	Young's modulus	300E3	kPa
	Poisson's ratio	0.44	
	Buoyant unit weight	11	kN/m ³
	Maximum initial yield cohesion	30	kPa
	Mohr-Coulomb peak friction angle	55	degrees
	Dilation angle	50	degrees
	Initial coefficient of lateral earth pressure	1.0	
Concrete pile	Young's modulus	24E6	kPa
	Poisson's ratio	0.28	
	Unit weight	24	kN/m ³
Interface – fill	Coefficient of interface friction	0.8	
	Allowable elastic slip	0.1	mm
Interface – oil sand	Coefficient of interface friction	1.1	
	Allowable elastic slip	0.1	mm

values. The coefficients of pile-oil sand interface friction are higher than those of concrete-sand interface (0.7-0.8) reported by Gómez *et al.* (2008) because oil sand has a higher peak friction angle. No dilation at the interface was allowed in the FE simulations.

In order to simulate the pile behaviour prior to and during loading, three steps were applied to the finite element model. Firstly, the “geostatic” step was used to obtain the initial vertical and horizontal effective stress state in the soil. The geostatic step ensured that the initial stress state was within the yield surface. The second step consisted of removing the soil and placing concrete into the excavated pile hole. This step simulated the change in the initial stresses at the pile-soil interface, i.e., residual stresses due to the weight of concrete. The third step involved application of the vertical load to the top of the pile in small increments.

A major difficulty when modeling an elasto-plastic soil with frictional contact and large deformations is the strong nonlinearities in obtaining a stable solution. Eigenbrod *et al.* (2005) recommended that for a jacked-in pile an optimal mesh size adjacent to the pile be in the range of one quarter to one-half the diameter of the pile. For cast-in-place pile, the strains on the soil are considerably less since the pile is not pushing the soil out of the way during installation and therefore a slightly finer mesh was used. A mesh approximately one-fifth the pile diameter around and below the pile with gradually increasing in size away from the pile, was used. This mesh

density tended to provide a reasonably accurate solution unbiased by large elements but with a relatively quick solution convergence rate. In this study, the load was applied in small increments so that the pile displacement was limited to 0.1% of the shaft diameter in each increment.

For the initial study to gain an understanding of the behaviour of the system, a linear elastic soil model was first used (i.e., without plastic straining). After the linear elastic analysis, an elasto-plastic soil model, which captures shear dilation and softening behaviour, was implemented. In addition, parametric studies were performed on selected parameters, such as in situ stress coefficient, elastic constants, and dilation angle, to distinguish the effect of varying values on the results of the model (Barr 2011). Only results of two cases (linear elastic and Mohr-Coulomb elasto-plastic models) are presented in this paper for performance evaluation of bored cast-in-place concrete pile in oil sand.

3.4 Results from numerical analyses

Results on pile-soil interaction of linear elastic (LE) and Mohr-Coulomb elasto-plastic (MC-EP) cases are included in Figs. 3 to 7 for comparison. It is of importance to understand that there exist some uncertainties in interpretation of field data including shaft resistance, end bearing resistance and top-down load. The average shaft resistances shown in Figs. 3 and 4 were calculated directly using the measurement data from the O-cell and strain gauges in the pile. Thus, the uncertainty is only associated with the accuracy of the measurement devices. For the end bearing resistances shown in Fig. 5, the shaft resistance at the 1.34-m section below the O-cell was estimated based on the extrapolation of Fig. 4, which might result in some uncertainties in estimation of end bearing resistance. There are also some assumptions and limitations embedded in the interpretation method (Lee *et al.* 2008) used in construction of the top-down load curves shown in Figs. 6 and 7. Therefore, we need to examine on the overall performance of each finite element model, rather than specific behaviour.

The average mobilized shaft resistances at the selected depth intervals of 3-6 m (or an average depth interval of 4.5 m, oil sand fill) and 6-8.8 m (or an average depth interval of 7.4 m, in situ oil sand) are compared to those predicted by the LE and MC-EP models in Figs. 3 and 4, respectively. In general, the LE model shows a bilinear response, i.e., the shaft resistance increases with increasing displacement. The vertical load in the pile causes a relative displacement at the pile-oil sand interface and an outward displacement of the pile against the surrounding oil sand. Both effects cause increases in the shaft resistance. The initial linear portion is mainly dominated by the response or stiffness of the concrete pile-oil sand interface. According to the interface model illustrated in Fig. 9, the estimated available maximum shear resistances at depths of 4.5 m and 7.4 m are 55 kPa and 90 kPa, respectively, at a relative displacement or slip of 0.1 mm. These estimated values are consistent with the “yielding” points of 50 kPa and 95 kPa predicted by the LE model. The maximum elastic slip for full shear mobilization at the interface is 0.1 mm. The LE model predicts that the full mobilization occurs at a 1-mm shaft displacement. This shaft displacement is much larger than the value of 0.1 mm because the surrounding oil sand also moves downwards with respect to the loaded pile due to the dragging effect. After the interface has achieved its maximum shear resistance, the increase in the shaft resistance is reduced to a lower rate, and derived from the confinement provided by the surrounding oil sand. The pile subject to compression displaces outwards against the surrounding oil sand due to the Poisson’s effect of the compressed pile. This creates an increase in the normal stress against the soil, effectively increasing the shearing resistance (Goodman 1989). The increase in shaft resistance is governed by

the Poisson's ratio of the concrete and the stiffness or Young's modulus of the surrounding oil sand. Results of parametric studies conducted by Barr (2011) demonstrate that the larger the Young's modulus of the oil sand is, the higher the shaft resistance developed. The variation of the Poisson's ratio of the oil sand has no discernable effect on the results, which is consistent with the studies performed by Randolph *et al.* (1978). Since the LE model assumes constant values in Poisson's ratio of concrete and Young's modulus of oil sand, thus the latter portion of the shaft resistance versus pile displacement curve is also linear.

The MC-EP model displays a similar trend in the mobilized shaft resistance versus pile displacement plot as the LE model does. The initial portion is due to the interaction at the interface between the concrete and oil sand, similar to what happens in the LE model. The latter portion is controlled by the Poisson's effect of the compressed pile and shear dilation of oil sand adjacent to the interface. The amount of shear dilation is controlled by the extent of the plastic shear zone and the dilation rate or angle. Since the plastic shear zone is limited to the narrow regions adjacent to the interface and a constant dilation angle or rate is assumed in the MC-EP model, the radial expansion induced by the shear dilation against the surrounding oil sand is approximately linearly proportional to the applied load. As the surrounding oil sand outside the plastic shear zone behaves linear elastic, the MC-EP model also predicts a linear response at the latter portion of the shaft resistance versus pile displacement plot. The MC-EP model displays no hardening with pile displacement as the field measurements tend to (Figs. 3 and 4). This behaviour may be explained by the fact that the MC-EP model assumes a constant dilation rate defined by the dilation angle whereas the dilation rates observed in the drained triaxial compression tests are stress and strain-dependent as shown in Fig. 8. In addition, the Young's modulus of the oil sand used in the MC-EP model was assumed constant, but the oil sand material displays stress-dependent modulus. If the stress-dependent modulus and variable dilation rate were implemented in the plastic model, the matching between the field monitoring and numerical simulation would be improved. The matching for the initial portions of the response curves at 7.5-m interval shown in Fig. 4 could also be enhanced by adjusting the stiffness of the interface between the concrete pile and oil sand, i.e., the allowable elastic slip at 7-m interval could be less than 0.1 mm.

From Figs. 3 and 4, the LE model under-predicts the mobilized shaft resistance as compared to the interpreted field data. In addition, the pile end bearing resistance predicted by the LE model is much larger than that observed in the field (Fig. 5). Due to this compensation effect between the shaft and end bearing resistances, the top-down load curve obtained from the field measurement and LE model are comparable as shown in Fig. 6. The MC-EP model performs better than the LE model in matching the shaft shear resistance and end bearing resistance of test pile load A2 as illustrated in Figs. 3 to 6. Fig. 7 shows clearly that the MC-EP model yields a better matching than the LE model in terms of the mobilized shaft resistance along the pile length and the end bearing capacity. However, the top-down load displacement curve predicted by MC-EP model is slightly stiffer than that predicted by the linear elastic model and the constructed curve of test pile A2 (Fig. 6). This may be attributed to the fact that in the MC-EP model the yielded oil sand continues to dilate under shear. It is of practical interest to note that to match the results of the entire O-cell test in test pile load A2, the loading modulus is different from the unloading. The plastic model should consist of a yield cap capturing the yielding during the primary loading path, which is beyond the scope of this paper.

Fig. 11 plots the vertical and radial displacements of the surrounding oil sand induced by the maximum pile load at 7.4 m depth predicted by the LE model. The downward movement of the pile drags the surrounding oil sand by the shear interaction. At the interface, the pile toe

displacement is about 14.9 mm (Fig. 5) and the oil sand displacement is 3.4 mm (Fig. 11(a)). The relative slip is 11.5 mm indicating the full shear resistance mobilization at the interface (DeJong *et al.* 2006). From Fig. 11(b), the oil sand experiences a small radial expansion of 0.05 mm at the interface due to the pile radial expansion under axial compression. This radial expansion increases the radial confining stress thereby increasing the shaft resistance (Lehane and White 2005). Beyond this small radial expansion zone, the radial displacement becomes negative, i.e., moving inward toward the pile centre. This inward movement is due to the drag action of the displaced pile causing the surrounding oil sand moving downward. The vertical and radial displacement profiles predicted by the MC-EP model are different from those predicted by the LE model (Fig. 11). The MC-EP model shows a marked increase in the vertical settlement due to pile load as compared to

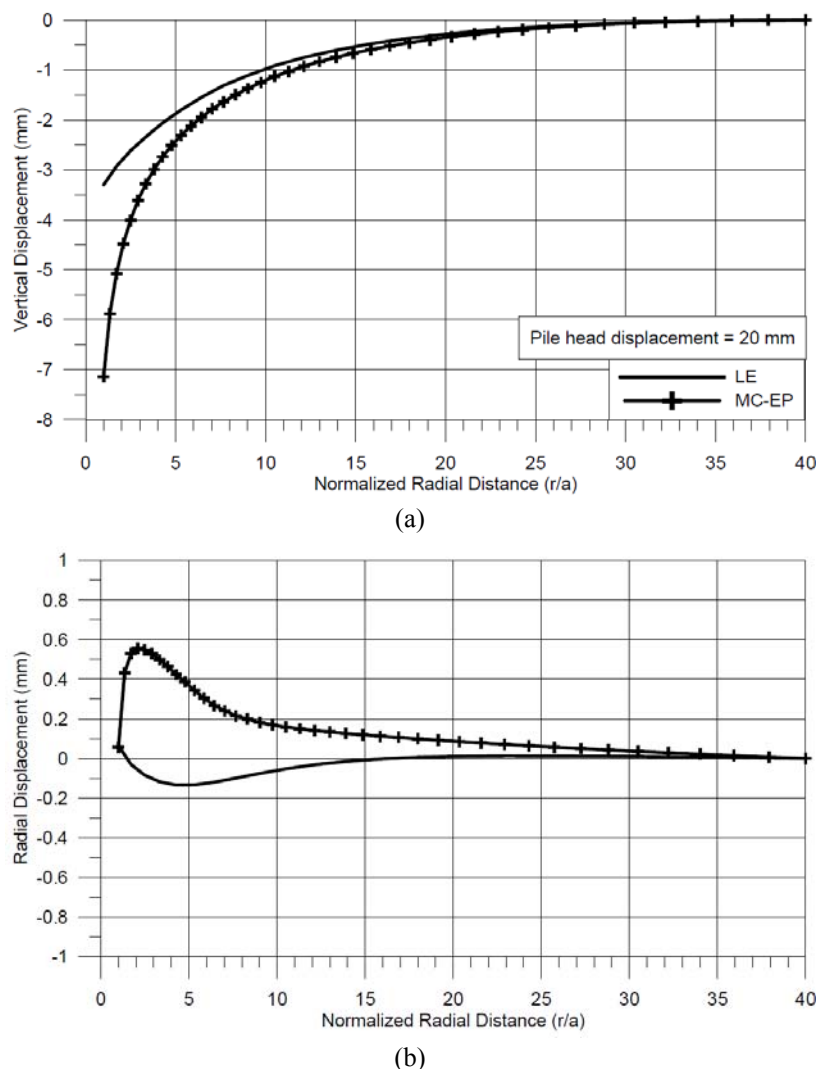


Fig. 11 (a) Vertical displacement versus normalized radial distance and (b) Radial displacement versus normalized radial distance at depth of 7.4 m (LE: linear elastic; MC-EP: elasto-plastic cases)

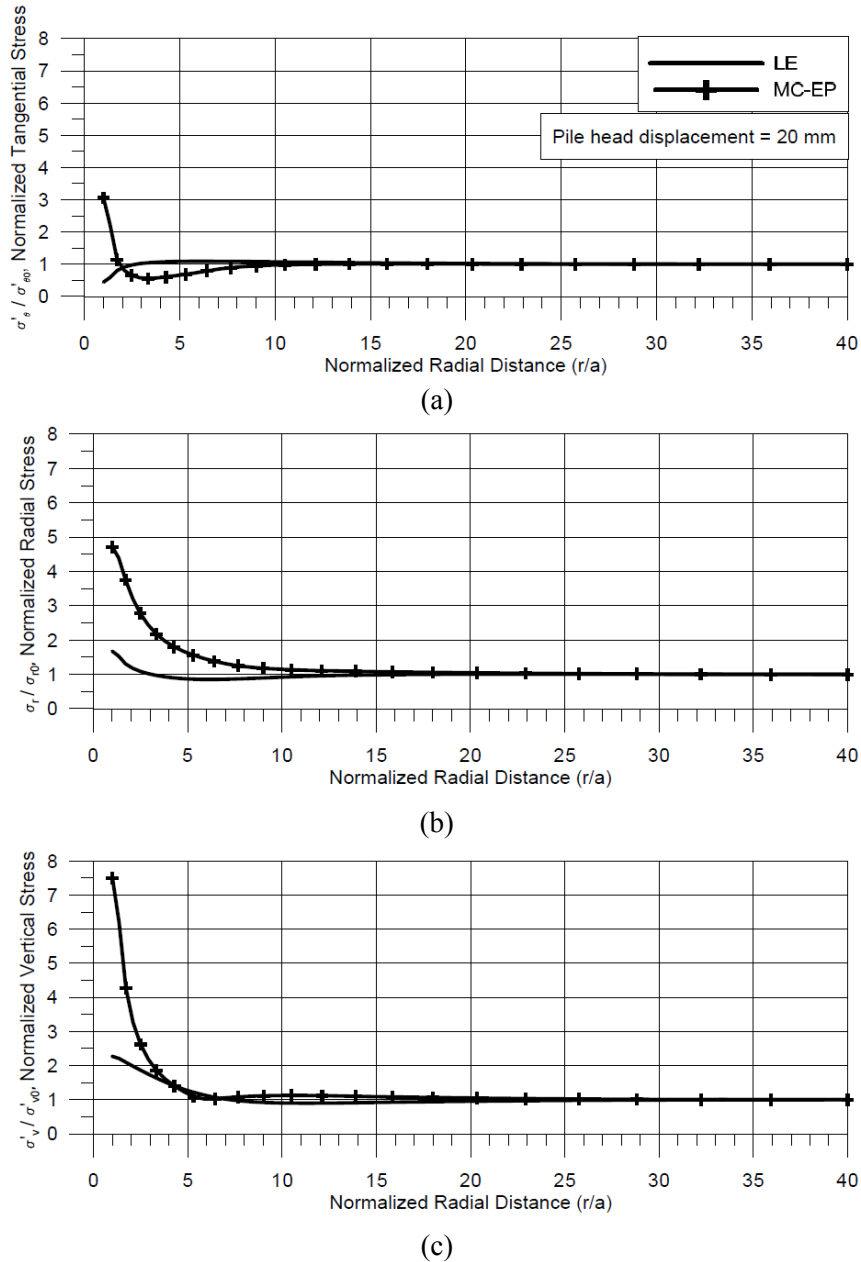


Fig. 12 (a) Normalized tangential stress versus normalized radial distance, (b) Normalized radial stress versus normalized radial distance, (c) Normalized vertical stress versus normalized radial distance at depth of 7.4 m (LE: linear elastic; MC-EP: elasto-plastic cases)

the LE model because plastic deformations are allowed and considered in the MC-EP model. The MC-EP model predicts that the radial displacements in the surrounding oil sand are all positive, i.e., the oil sand displaces outward in the radial direction. The oil sand at the pile interface expands

due to the pile radial expansion under axial compression whereas the surrounding oil sand moves outward due to the shear dilation of the sheared oil sand.

Fig. 12 compares the normalized tangential, radial and vertical stress distributions at 7.4-m depth in the surrounding oil sand at the maximum pile load predicted by the LE and MC-EP models. The LE model predicts that the oil sand experiences a 55% decrease, 70% increase, and 125% increase in tangential, radial, and vertical stresses, respectively, as compared to the initial in situ stresses. The induced Beta-coefficient is 1.7, which is much lower than that observed in the pile test. The influence zone is only about 1 to 6 times the pile radius. Beyond this disturbed zone, the stresses remain unaffected by the pile load. The MC-EP model shows significant differences in stress distributions near the concrete pile as compared to the LE model. There are significant increases in three stresses (tangential, radial and vertical) at the pile interface. These three stresses are not the principal stress components as there are induced shear stresses due to the pile load. However, it can be seen that the soil yielding or failure at the pile interface are governed by the stress difference between the vertical and tangential stress components. The radial stress is the intermediate stress component. This stress redistribution due to pile loading cannot be predicted using a 2D cavity expansion model in which the radial and tangential stresses are the major and minor principal stresses respectively, with the vertical stress being as the intermediate principal stress. The Beta-coefficient based on the radial stress is 4.7, which is consistent with the measured value from the test pile. For the vertical and radial stresses, the maximum values occur at the pile interface and they gradually decrease to their initial in situ values along the radial distance. The tangential stress also shows a similar trend but, it drops below its initial in situ value at a radial distance of about 2 pile radii, i.e., there is a zone of stress reduction in tangential direction due to shear dilation.

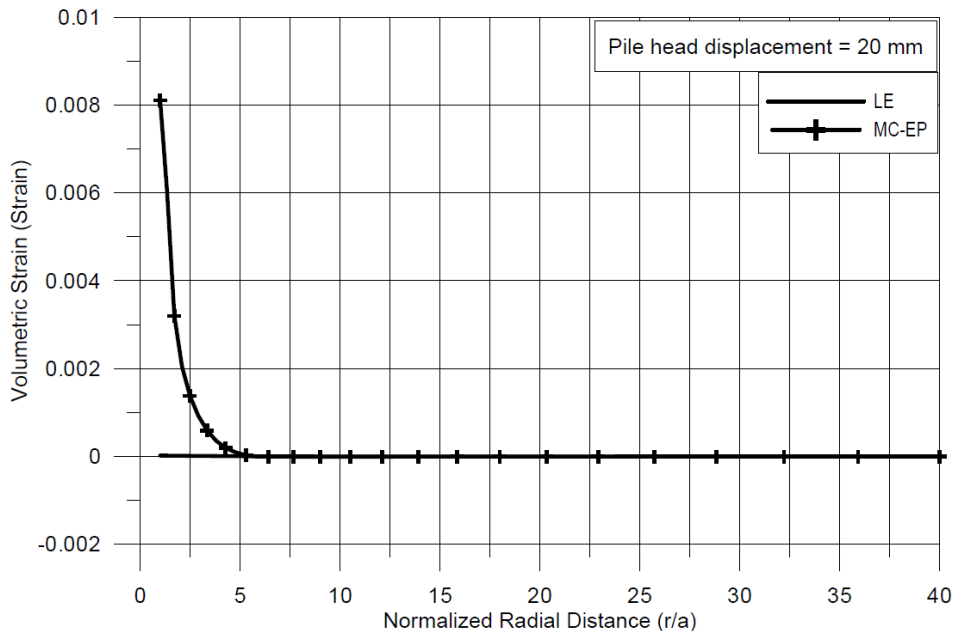


Fig. 13 Volumetric strain versus normalized radial distance at depth of 7.4 m (LE: linear elastic; MC-EP: elasto-plastic cases)

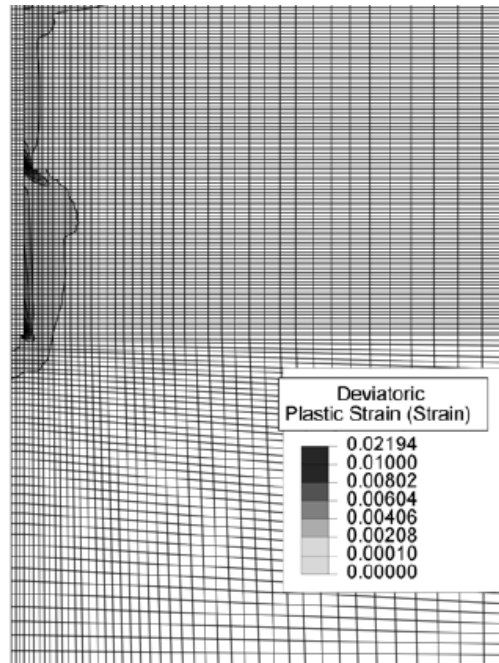


Fig. 14 Formation of plastic zone around the pile (pile head displacement = 20 mm)

Fig. 13 plots the volumetric strain distribution at 7.4-m depth in the surrounding oil sand at the maximum pile load predicted by the LE model. The induced mean effective stress is small. Thus, the induced volumetric strain is insignificant. For the MC-EP case, there is a volumetric strain occurring due to shear dilation. The maximum volumetric strain is about 0.008 at the pile face. According to the stress-strain curves shown in Fig. 8, the stress regime in the oil sand is within the pre-peak domain, and post-peak softening may not occur in such case.

Fig. 14 presents the plastic or yield zone in terms of plastic deviatoric strain around the pile predicted by the MC-EP model. Note that there is a strain concentration at a depth of 5 m, which corresponds to a contrast in stiffness and strength parameters in the two materials. The extent of the yield zone in the in situ oil sand is larger than that in the oil sand fill.

Results shown in Figs. 11 to 14 explain why the LE and MC-EP models could yield comparable top-down load versus pile head displacement curves, but very different behaviour in mobilization of pile shaft and end bearing resistances.

4. Conclusions

Results from pile load tests show that high shaft shear resistances were mobilized on straight cast-in-place concrete piles founded in oil sand. The ratios of mobilized shear stress to vertical effective stress shear stress or Beta coefficients are much higher than those recommended in Canadian Foundation Engineering Manual. Finite element simulations based on linear elastic and elasto-plastic models were used in analyzing the in situ behaviour of cast-in-place concrete pile in oil sand to determine important factors contributing to development of such high shaft resistance.

Pile load induces shear deformation around the pile forming a yielded zone. The yielding around the pile is controlled by the stress difference between the vertical (major) and tangential (minor) stress components as the radial stress is the intermediate component. Due to the interlocked structure of the oil sand, high shear dilation is developed within the yield zone, thereby causing an outward radial expansion against the surrounding oil sand. Because of the high stiffness of the oil sand, the increase in the radial or horizontal stress is significant resulting in high mobilized shear stress along the pile shaft. Thus, the pile resistance of the cast-in-place pile derived from the end bearing is comparatively low in this study.

Acknowledgements

The authors appreciate the supports from Thurber Engineering Limited, University of Calgary, and Natural Sciences and Engineering Research Council of Canada (NSERC).

References

- ABAQUS (2009), ABAQUS standard user's manual, Version 6.9, Hibbitt, Karlsson and Sorensen, Pawtucket, R.I.
- Agar, J.G., Morgenstern, N.R. and Scott, J.D. (1987), "Shear strength and stress strain behaviour of Athabasca oil sands at elevated temperatures", *Can. Geotech. J.*, **24**(1), 1-10.
- API (2002), American Petroleum Institute (API), API Recommended Practice for Planning, Designing, and Constructing Fixed Offshore Platforms, Working Stress Design, 21st Edition, (RP 2AWSD), American Petroleum Institute.
- ASCE (1984), "Guidelines for the seismic design of oil and gas pipeline systems", *Committee on Gas and Liquid Fuel Lifelines, American Society for Civil Engineering (ASCE)*, New York.
- ASTM (2007), Standard test methods for deep foundations under static axial compressive load, ASTM standard D1143/D1143M-07, *In Annual Book of ASTM Standards*, American Society for Testing and Materials (ASTM), West Conshohocken, Philadelphia, Pennsylvania.
- Barr, L. (2011), Finite element analysis of straight shaft cast-in-place concrete pile set in oil sand", M. Eng. Thesis, Department of Civil Engineering, University of Calgary, Calgary, Alberta.
- Bawden, W.F. (1983), "Hydraulic fracturing in Alberta tar sand formations, a unique material for in-situ stress measurements", *In Hydraulic Fracturing Stress Measurements*, National Academy Press, Washington, D.C., 91-103.
- Bolton, M.D. (1986), The strength and dilatancy of sands", *Geotech.*, **36**(1), 65-78.
- Burland, J.B. (1973), "Shaft friction piles in clay – a simple fundamental approach", *Ground Eng.*, **6**(3), 30-42.
- CGS (2006), "Canadian Foundation Engineering Manual", *Can. Geotech. Soc.*, 4th Edition, Bi-Tech Publisher Ltd. Richmond, British Columbia.
- Carrigy, M.A. (1966), "Lithology of the Athabasca Oil Sands", Bulletin 14, Research Council of Alberta, Edmonton, Alberta.
- Clementino, R., Tweedie, R., Sobkowicz, J.C., Workman, C. and Sisson, R. (2006), "High capacity cast-in-place concrete pile load tests at CNRL's oil sand plant site near Fort McMurray", Alberta, 59th *Canadian Geotechnical Conference*, Vancouver, British Columbia.
- Clementino, R., Tweedie, R., Workman, W.C. and Barr, L.A. (2011), High capacity cast-in-place concrete piles in oil sand near Fort McMurray, Alberta, Special Technical Publication Honouring Dr. Bent Fellenius, *J. Geotech. Eng. ASCE*. [In Press]
- DeJong, J.T., White, D.J. and Randolph, M.F. (2006), "Microscale observation and modelling of

- soil-structure interface behaviour using particle image velocimetry”, *Soils Found.*, **46**(1), 15-28.
- Dusseault, M.B. and Morgenstern, N.R. (1978), “Shear strength of Athabasca oil sands”, *Can. Geotech. J.*, **15**(2), 216-238.
- Dusseault, M.B. (1979), “Shear state and hydraulic fracturing in Athabasca oil sands. Journal of Canadian Petroleum Technology”, *Geotech. J.*, **16**(1), 19-27.
- Dusseault, M.B. and Morgenstern, N.R. (1979), “Locked sands”, *Quarter. J. Eng. Geol.*, **12**(2), 117-131.
- Eigenbrod, K.D., Sheng, D. and Wiggers, P. (2005), “Finite element analysis of pile installation using large-slip”, *Comp. Geotech.*, **32**(1), 17-26.
- Fellenius, B.H. (1999), Bearing capacity of footings and piles - A delusion?, *Proceedings of the Deep Foundation Institute Annual Meeting*, Dearborn, Michigan, October.
- Fellenius, B.H. (2009), The red book — basics of foundation design, Revised electronic Edition, Available from <http://www.fellenius.net>.
- Gómez, J.E., Filz, G.M., Ebeling, R.M. and Dove, J.E. (2008), “Sand-to-concrete interface response to complex load paths in a large displacement shear box”, *Geotech. Test. J.*, **31**(4), 1-12.
- Goodman, R.E. (1989), *Introduction to rock mechanics*, 2nd Edition, John Wiley and Sons, Berkeley, California.
- Lehane, B.M. and White, D.J. (2005), “Lateral stress changes and shaft friction for model displacement piles in sand”, *Can. Geotech. J.*, **42**(4), 1039-1052. doi:10.1139/t05-023.
- Lee, J.S. and Park, Y.H. (2008), “Equivalent pile load-head settlement curve using a bi-directional pile load test”, *Comp. Geotech.*, **35**(2), 124-133.
- Menétrey, Ph. and Willam K.J. (1995), “Triaxial failure criterion for concrete and its generalization”, *ACI Struct. J.*, **92**(3), 311-318.
- Osterberg, J.O. (1984), “A new simplified method for load testing drilled shafts”, *Found. Dril. ASDC*, **23**(6), 9.
- Osterberg, J.O. (1998), “The Osterberg load test method for drilled shaft and driven piles - The first ten years. Seventh International Conference and Exhibition on Piling and Deep Foundations”, *Deep Found. Inst. Vienna*, Austria.
- Randolph, M.F. and Wroth, P. (1978), “Analysis of vertically loaded piles”, *J. Geotech. Eng. ASCE*, **104**(GT 12), 1465-1488.
- Rowe, P.W. (1962), The stress-dilatancy relation for static equilibrium of an assembly of particles in contact, *Proceedings of Royal Society*, **269A**, 500-527.
- Said, I., De Gennaro, R. and Frank, R. (2009), “Axisymmetric finite element analysis of pile load tests”, *Comp. Geotech.*, **36**(5), 6-19.
- Samieh, A.M. and Wong, R.C.K. (1997), “Deformation of Athabasca oil sand at low effective stresses under varying boundary conditions”, *Can. Geotech. J.*, **34**(6), 985-990.
- Samieh, A.M. and Wong, R.C.K. (1998), “Modelling the response of Athabasca oil sand in triaxial compression tests at low pressure”, *Can. Geotech. J.*, **35**(2), 395-406.
- Sharma, H.D., Harris, M.C., Scott, J.D. and McAllister, K.C. (1986), “Bearing capacity of bored cast-in-place piles on oil sand”, *J. Geotech. Eng. ASCE*, **112**(12), 1101-1116.
- Sobkowitz, J.C. and Harris, M.C. (1977), “Engineering behaviour of oil sand. The oil sands of Canada and Venezuela”, *Can. Inst. Mining Metallurgy, Special Volume 17*, 271-283.
- Terzaghi, K. (1943), *Theoretical soil mechanics*, John Wiley and Sons, Inc., New York.
- Wijewickreme, D., Karimian, H. and Honegger, D. (2009), “Response of buried steel pipelines subject to relative axial soil movement”, *Can. Geotech. J.*, **46**(7), 735-752.
- Wong, R.C.K. (1999), “Mobilized strength components of Athabasca oil sand in triaxial compression”, *Can. Geotech. J.*, **36**(4), 718-735.
- Veiskarami, M., Eslami, A. and Kumar, J. (2011), “End-bearing capacity of driven piles in sand using the stress characteristics method: analysis and implementation”, *Can. Geotech. J.*, **48**(12), 1570-1586.